J Therm Anal Calorim (2014) 117:109–122
DOI 10.1007/s10973-014-3669-7

Graphene oxide improved thermal and mechanical properties of electrospun methyl stearate/polyacrylonitrile form-stable phase change composite nanofibers

Huizhen Ke · Zengyuan Pang · Yunfei Xu · Xiaodong Chen · Jiapeng Fu · Yibing Cai · Fenglin Huang · Qufu Wei

Received: 11 September 2013 / Accepted: 21 January 2014 / Published online: 18 February 2014

Abstract In the present work, a novel PAN-based form-stable composite phase change materials with the methyl stearate (MES) encapsulated in the supporting matrices of polyacrylonitrile (PAN) nanofibers were fabricated through electrospunning for the storage and retrieval of thermal energy. Influences of graphene oxide (GO) addition on the chemical properties, structural morphologies, mechanical properties, thermal energy storage properties, thermal stability, and thermal energy storage/retrieval rates of electrospun MES/PAN/GO phase change composite nanofibers were systematically investigated by FT-IR, FE-SEM, tensile testing, DSC, TG, and measurement of melting/freezing times, respectively. The results revealed that the incorporation of GO effectively enhanced the mechanical properties, thermal stability, as well as heat storage and release rates of the phase change composite nanofibers. The averaged tensile strength of electrospun MES/PAN/GO phase change composite nanofibers increased significantly by 573 % with 10 mass% loading of GO, while elongation at break had a maximum 107 % increment when adding 3 mass% of GO. The DSC results indicated that the electrospun PAN-based phase change composite nanofibers with various GO loadings had suitable phase transition temperatures with the latent heat ranging from about 92 to 109 kJ kg^{-1} and exhibited good thermal reliability in terms of DSC measurements during 50 melting-freezing cycles. Moreover, the melting and freezing time were significantly decreased about 44 and 43 % for the MES/PAN/GO5, as well as 59 and 64 % for the MES/PAN/GO10 after introducing the GO into the composite nanofibers systems.

Keywords Form-stable PCMs · Graphene oxide · Polyacrylonitrile · Methyl stearate · Mechanical properties · Thermal conductivity

H. Ke · Z. Pang · Y. Xu · X. Chen · J. Fu · Y. Cai · F. Huang · Q. Wei (✉)
Key Laboratory of Eco-Textiles, Ministry of Education, Jiangnan University, Wuxi 214122, Jiangsu, China
e-mail: qfwei@jiangnan.edu.cn

Introduction

Over the recent decades, there has been increasing interest in latent heat storage technology using phase change materials (PCMs), which has been successfully applied in numerous fields of solar energy systems, energy efficient buildings, smart air-conditioning, temperature-adaptable greenhouses, space and water heating, industrial waste heat recovery, cooling of engines, medical application, thermal insulation, homothermal textiles, and solar thermal power plant [1–7] because of the distinctive advantages such as high heat storage density, narrow temperature variation from reserve to release thermal energy, much less insulation required, lower vapor pressure, and volume change [7, 8].

As a new type organic solid–liquid PCMs, fatty acid esters, which can storage or retrieval large amounts of latent heat and adjust temperature as they change from one physical state to another, has drawn a great deal of attention due to its non-toxic, non-corrosive, high enthalpy, a narrow temperature range during the phase transition, low cost, good thermal, and chemical properties with little supercooling or phase segregation [9–11]. The preparation and thermal properties of some fatty acid esters have been studied for the applications related to the store and retrieval of thermal energy in recent years. For example, Aydin et al. [9] reported the synthesis of a series of high-chain fatty acid esters of 1-tetradecanol (myristyl alcohol) by

esterification reaction, and characterized these substances by FT-IR, DSC, and TG measurements. Their results showed that these synthesized esters were favorable for low-temperature heat transfer applications with superior thermal properties and reliability. Sari and coworkers [10] reported synthesis, characterization and thermal properties of a series of stearic acid esters as novel solid–liquid PCMs, and revealed that the synthesized esters have significant energy storage potential due to their satisfactory thermal properties, good thermal reliability, and thermal conductivities. Sari et al. [11] also investigated the synthesis, thermal energy storage properties and thermal reliability of some fatty acid esters with glycerol as novel solid–liquid phase change energy storage materials, and indicated that the synthesized esters can be considered as a potential PCMs for thermal energy storage. Nevertheless, the leakage and poor thermal conductivity of organic solid–liquid PCMs (e.g., fatty acid esters) probably limit their direct applications in some areas. It is thereby essential to fabricate form-stable PCMs with an enhanced thermal performance to broaden their application. Currently various supporting materials have been selected to solve this leakage problem including polymethyl methacrylate [12], high-density polyethylene (HDPE) [13], polyethylene [14], polypropylene [15], ultra high molecular mass polyethylene (UHMWPE) [16], polyethers [17], PnBMA [18], diacetate cellulose (CDA) [19], poly(acrylic acid) (PAA) and poly(ethylene-co-acrylic acid) (EcoA) [20], polyurethane [21], poly(methylmethacrylate-co-divinylbenzene) [P(MMA-co-DVB)] [22], polyamide 6 (PA6) [23], polyethylene terephthalate (PET) [24], attapulgite [25], silicon dioxide [26], diatomite [27], halloysite nanotube [28], expanded perlite [29], vermiculite [30], expanded graphite [31], and carbon nanotubes [32] etc. Moreover, the low thermal conductivity of PCMs, which makes the rates for storing and releasing of thermal energy during the melting and crystallization processes to be slow, had also been overcame by adding high thermal conductivity substances into solid–liquid PCMs like silicon dioxide [26], expanded graphite [27–31], carbon nanotubes [32, 33], carbon fibers [33], and Ag nanowires [34] etc. These additives can effectively improve the overall heat transfer and/or diffusion properties of PCMs.

Graphene oxide (GO), a two-dimensional (2D) single-layered carbon material, has recently attracted extensive attention owing to its unique structure, large specific surface area, superior electronic conductivity, high thermal conductivity, excellent mechanical properties, and low cost. There are a large number of oxygen-containing functional groups attached on the basal planes and edges of GO sheets such as hydroxyl, epoxide, carboxyl, and carbonyl groups, which could allow homogeneous dispersion of GO nanosheets in water or different solvents and effectively improve interfacial interaction and compatibility between GO and polymeric matrix [32–51]. Recently, a variety of GO-based polymer composites (e.g., Nylon-6 [36], polysaccharide [37], poly(vinyl alcohol) [38], polyamide and polyphenylene [39], poly(arylene ether nitrile) [40], polybenzimidazole [41], carboxylated acrylonitrile butadiene rubber [42], silicone [43], Polyimide [44], polyurethane [45], polymethyl methacrylate [46], polypropylene [47], acrylic resins [48], polypyrrole [49], polyaniline [50], and epoxy [51],) have been extensively investigated to improve their mechanical [36–45], thermal stability [38–46], thermal conductive properties [42–44], electrical [46–50], electrochemical [49, 50], biocompatibility [37, 50], and tribological [51] properties.

Methyl stearate (MES) is a favorable fatty acid ester with the attractive advantages of high energy storage capacity, suitable phase change temperature, good thermal reliability and chemical stability, better odor, non-corrosivity, and cost-effective, which can be considered as potential organic solid–liquid PCM for storage and retrieval of thermal energy. Polyacrylonitrile (PAN) is an important engineering polymer material that has been widely used to produce electrospun nanofiber membranes for many applications due to its good spinnability, attractive structural and mechanical characteristics, outstanding chemical, and thermal stability property, as well as low cost [52].

However, to the best of our knowledge, there have been no previous reports on the preparations of PAN-based form-stable PCMs with PAN acting as polymer supporting materials. Furthermore, the study on the preparations of form-stable PCMs incorporating MES, which was chosen as solid–liquid PCM, has also never been reported. In this study, therefore, the PAN-based form-stable phase change composite nanofibers were prepared by encapsulating MES into PAN nanofibers matrix using simple electrospinning method. In addition, in order to enhance the mechanical properties, thermal stability and thermal conductivity, electrospun MES/PAN/GO phase change composite nanofibers with various contents of GO were also fabricated, in which the GO was selected as heat transfer/diffusion promoters and could also act as supporting material by interfacial interactions, capillary force, and surface tension. The effects of GO loading on the chemical properties, structural morphologies, mechanical strength, thermal energy storage properties, thermal stability and thermal conductivity, properties of electrospun MES/PAN/GO phase change composite nanofibers were systematically characterized by fourier transform infrared (FT-IR) spectra, field emission scanning electron microscope (FE-SEM), tensile testing, differential scanning calorimetry (DSC), thermogravimetric (TG) analyses, and measurement of melting/freezing times, respectively.

Experimental

Materials

The PAN powder (PAN, $M_w = 50{,}000$–$60{,}000$) was purchased from Aldrich. The chemicals of methyl stearate (MES, $CH_3(CH_2)_{16}COOCH_3$) and *N*, *N*-dimethyl formamide (DMF) were supplied by the Sinopharm Group Chemical Reagent Co., Ltd. (Shanghai, China). The GO was obtained from the Nanjing Pioneer Nanomaterials Technology Co., Ltd. (Nanjing, China). All of the chemicals were used as received without further purifications.

Fabrication of the MES/PAN/GO phase change composite nanofibers

The GO were first dispersed in DMF solvent with different mass ratios [W_{GO}:($W_{MES} + W_{PAN} + W_{GO}$)] of 1, 3, 5, and 10 mass% in a 100 W ultrasonic bath for 12 h at room temperature. The PAN at a concentration of 10 mass% (with respect to DMF) was then dissolved in the solution and stirred to obtain a uniform polymer solution at ~50 °C. Subsequently, the MES powder was added into the previously prepared solution with a fixed concentration (W_{MES}:$W_{PAN} = 1.2$:1). Thereafter, these spinning solutions were magnetically stirred to achieve the well-dispersed solutions for electrospinning. The codes of electrospun phase change composite nanofibers were referred to as MES/PAN/GO1, MES/PAN/GO3, MES/PAN/GO5, and MES/PAN/GO10, respectively.

Electrospinning solution was loaded into a 20 mL plastic syringe with a blunt-end stainless steel needle. The inside diameter of the metal needle was 0.3 mm. During electrospinning, the solutions were fed using a syringe pump purchased from the medical instrument Co. (Hangzhou, China) at a rate of 1 mL h^{-1}. The electrospun phase change composite nanofibers were collected as overlaid fibrous mats on the electrically grounded aluminum foil that covered the roller collector. The rotating speed of the roller was fixed at 100 rpm. The voltage applied between the spinner outlet and the roller collector was set at 18 kV, and the distance between the needle tip and the roller was set at 16 cm. In addition, the PAN nanofibers and MES/PAN phase change composite nanofibers were also electrospun for comparison. All electrospun samples were dried in a vacuum oven at room temperature for 24 h to remove the residual solvent.

Characterizations and evaluations

Fourier transform infrared spectroscopy

FT-IR spectra were obtained using a Nicolet iS10 FT-IR spectrometer (Thermo Fisher Scientific) with the wavenumber ranging from 400 to 4,000 cm^{-1}.

High-resolution transmission electron microscope

A HR-TEM (JEOL-2100) was used to examine the morphology of pure GO nanosheets. The sample was prepared by first dispersing the GO in anhydrous ethanol, and then the dispersion was dropped on copper grid. Thereafter, the sample was dried at room temperature under vacuum before observation.

Field emission scanning electron microscopy

The morphologies of electrospun nanofibers were observed with a Hitachi S-4800 FE-SEM at an accelerating voltage of 1 kV. Prior to imaging with the FE-SEM, the sample was sputter coated with gold to avoid charge accumulations.

Mechanical testing

Mechanical property testing was performed by using a computer control electronic universal testing machine (KDII-0.05) at room temperature. The samples were cut along the revolving direction of the drum with lengths of 100 mm and widths of 10 mm. The thicknesses of the membranes were accurately measured using a digital micrometer. A crosshead speed of 50 mm min^{-1} was used for all the specimens tested. The reported tensile strengths and elongations at break were the average of at least ten specimens.

Differential scanning calorimetry

The phase change temperatures and enthalpies of the MES powder and electrospun phase change composite nanofibers were determined by a DSC-Q200 thermal analyzer with the scanning rate of 8 °C min^{-1} over the temperature range of 0–100 °C. The DSC analyses were carried out under a constant nitrogen atmosphere at a flow rate of 50 mL min^{-1}. About 5–10 mg sample was sealed in an aluminum pan for the measurement.

Thermogravimetry analyses

The thermal stability of the MES powder and electrospun phase change composite nanofibers was investigated by a thermogravimetric analyzer (TG-Q5000 thermo-analyzer instrument) under a constant stream of nitrogen with the flow rate of 25 mL min^{-1}. The about 10 mg specimen was heated from 25 to 800 °C using a linear heating rate of 10 °C min^{-1}. The precisions of measurements for temperature and mass during TG experiments were ±2.0 °C and ±2.0 %, respectively.

Thermal performance test

Thermal performance test was performed to investigate the effect of GO addition on thermal energy storage and retrieval rates of electrospun MES/PAN phase change composite nanofibers. Figure 1 shows the schematic of the experimental instrument for thermal energy storage and release performance measurement. The electrospun nanofibrous membranes with mass of about 5 g were first cut to pieces and put into sealed glass bottle. The thermocouple was then immersed into the center of the samples to monitor the internal temperature changes. Thereafter, the sealed bottle containing samples were put into the constant temperature water bath at 60 °C for the heating process. After the temperature reached balance, the samples were immediately subjected to cooling process in another constant temperature water bath at 10 °C. The temperature variations of the samples during these periods were automatically recorded by computer via data logger with a temperature measuring accuracy of ±2 °C at time intervals of 1 min. The conductivity measurements were repeated three times.

Results and discussion

Chemical structure

The FT-IR spectra of (a) original GO nanosheets, (b) electrospun PAN nanofibers, (c) pure MES powder, and (d) electrospun MES/PAN phase change composite nanofiber as well as (e) electrospun MES/PAN/GO5 phase change composite nanofibers are shown in Fig. 2. For the FT-IR spectrum of the GO nanosheets in Fig. 2a, there was a strong characteristic absorption peak at the wave numbers of about 3,368 cm^{-1}, which was assigned to –OH groups. It could be clearly seen that the GO nanosheets also had two characteristic absorption peaks at 1,715 cm^{-1} (C=O) and 1,405 cm^{-1} (C–OH) corresponding to vibration of carboxyl group. The strong absorption peaks at 1,217 cm^{-1}(C–O) and 1,043 cm^{-1} (C–O–C) were attributed to epoxy groups and alkoxy groups. Moreover, the 1,621 cm^{-1} (C=C) absorption band could be associated with the remaining sp^2 character [37, 39–41]. Figure 2b reveals that the positions of all peaks were consistent with the standard infrared spectrum of PAN. The typical absorption peak at about 2,242 cm^{-1} was ascribed to the stretching vibration of nitrile groups (–C≡N) in PAN molecular chains, as well as the characteristic peaks at 2,928 and 1,450 cm^{-1} were contributed to the asymmetrical and symmetrical bending vibrations of methylene groups ($–CH_2–$), respectively [52]. In the spectrum of the MES powder in Fig. 2c, there were two characteristic peaks corresponding to the stretching vibrations of C=O and C–O groups of the acyclic saturated ester at the wave numbers of 1,738 and 1,170 cm^{-1}, respectively. In addition, the absorption peaks at 2,917 and 2,842 cm^{-1}, respectively, represented the asymmetric and symmetric stretching vibrations of C–H bond. Besides these bands, the characteristic absorption peaks at about 1,468 and 724 cm^{-1} assigning to the CH_2 or CH_3 deformation vibration and the rocking vibration in $(–CH_2–)_n$ ($n \geq 4$) groups were also observed in the spectrum.

As shown in Fig. 2d, the FT-IR spectra of electrospun MES/PAN phase change composite nanofibers had no significant new characteristic peaks except the absorption bands belonging to the MES molecular and the PAN molecular, suggesting that there was no chemical reaction during the electrospinning process. Moreover, it could be found that the –C≡N absorption peak slightly shifted to

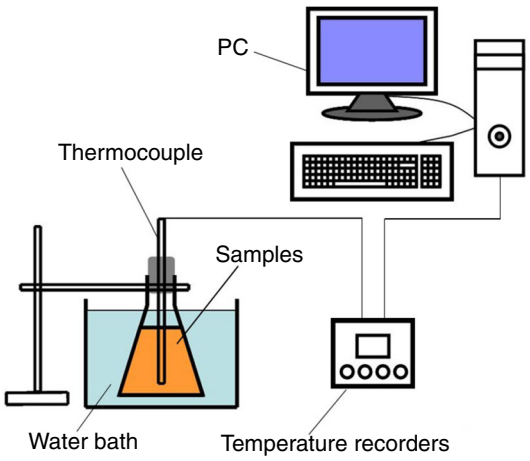

Fig. 1 Schematic diagrams of the experimental setup for thermal energy storage and release processes measurement

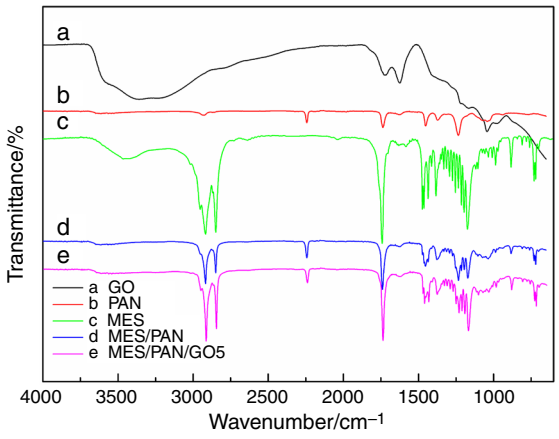

Fig. 2 FT-IR spectra of **a** pure MES powder, **b** pristine GO, **c** PAN nanofibers, **d** MES/PAN phase change composite nanofibers, and **e** MES/PAN/GO5 phase change composite nanofibers

2,239 cm^{-1}, while the relative intensity of absorption peaks regarding to the C–H bond stretching vibration of the MES molecular obviously decreased and also slightly shifted to 2,914 and 2,845 cm^{-1}, which could be account for the hydrogen interactions between PAN molecular and MES molecular. The characteristic absorption peaks in the FT-IR spectra of electrospun MES/PAN/GO phase change composite nanofiber were approximately similar with the spectrum of electrospun MES/PAN phase change composite nanofiber as shown in Fig. 2e. It could also be observed that the characteristic peaks of GO nanofibers could overlap with the absorption bands of PAN and MES in the composite nanofibers spectrum, indicating that the GO and MES/PAN had good compatibility in those composite nanofibers. Moreover, the peaks at 2,917, 2,842 and 1,738 cm^{-1}, respectively, regarding to the C–H and C=O groups from MES molecular were down shifted to 2,913, 2,841, and 1,734 cm^{-1}. Furthermore, the nitrile groups (–C≡N) of PAN molecular chain also slightly shifted to 2,237 cm^{-1} compared to that of pure PAN nanofibers. These observable frequency shifts of the main groups of electrospun MES/PAN/GO phase change composite nanofiber indicated the existence of the interface interaction after introducing the GO nanosheets into the composite nanofibers. It was believed that there were some hydrogen bonding interactions between the GO containing oxygen-containing functional groups (i.e., –OH, –COOH, and C=O groups), –C≡N of PAN, as well as C=O group of MES, which could effectively prevent the leakage of melted MES from the PAN/GO supporting matrices during the phase transition processes.

Morphology and structure

The TEM micrograph in Fig. 3 obviously reveals that the GO had nanosheet structures with some irregular corrugations and slightly folded edges, which was consistent with the result from previously reported literature [40, 46, 47]. In this paper, electrospun PAN nanofibers was chosen as the polymer supporting matrix of form-stable phase change composite nanofibers because PAN has not only excellent chemical resistance, as well as thermal stability and mechanical properties but also much higher melting point than that of MES. PAN can effectively prevent the leakage of the molten MES and help maintain the nanofibrous shape during the phase change processes [52]. The structural morphologies of electrospun PAN nanofibers, MES/PAN and MES/PAN/GO phase change composite nanofibers with different contents of GO are shown in Fig. 4. It was clearly seen from Fig. 4a that electrospun PAN nanofibers had quite uniform diameter distribution with smooth surface and cylindrical morphology structures. However, the image of Fig. 4b shows that the electrospun MES/PAN phase change composite nanofibers appeared to have coarse and wrinkled surfaces with shallow grooves, and the average fiber diameter (AFD) slightly increased when compared to that of pure PAN nanofibers, suggesting that the addition of MES affected morphological structure of composite nanofibers. Nonetheless, it was noticeable that the MES were well embedded and dispersed in three-dimensional network structures of composite nanofibers due to the polymer protection and supporting effect of PAN matrice.

As revealed in Fig. 4c–f, the electrospun MES/PAN/GO phase change composite nanofibers with various GO amounts were also randomly distributed to form the homogeneous nanofibrous mats. Apparently, the AFD of electrospun MES/PAN/GO phase change composite nanofibers was slightly lower than that of the MES/PAN composite nanofibers, which might be attributed to the increased conductivity of the electrospinning solution as a result of the incorporation of GO. Moreover, it could also be found that the electrospun MES/PAN/GO phase change composite nanofibers showed the similar rough surfaces structure and the conglutinations at some cross sites could be occasionally observed, indicating the formation of the strengthened interfacial adhesion. This may be contributed to the fact that the GO nanosheets, which have numerous oxygen-containing functional groups and presents the high specific surface area and crumpled surface textures with curling edges, could play a beneficial role in enhancing interfacial interaction with the MES and the PAN. It was also noteworthy that the GO nanosheets randomly distributing in the spin dopes, as well as in the phase change composite nanofibers could also act as the supporting material to absorb a certain amount of MES based on the capillary action and interfacial interaction. It is believed that there were three different possibilities of the MES

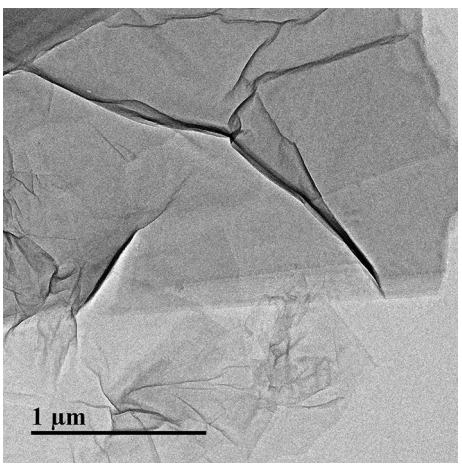

Fig. 3 TEM image of the GO nanosheets

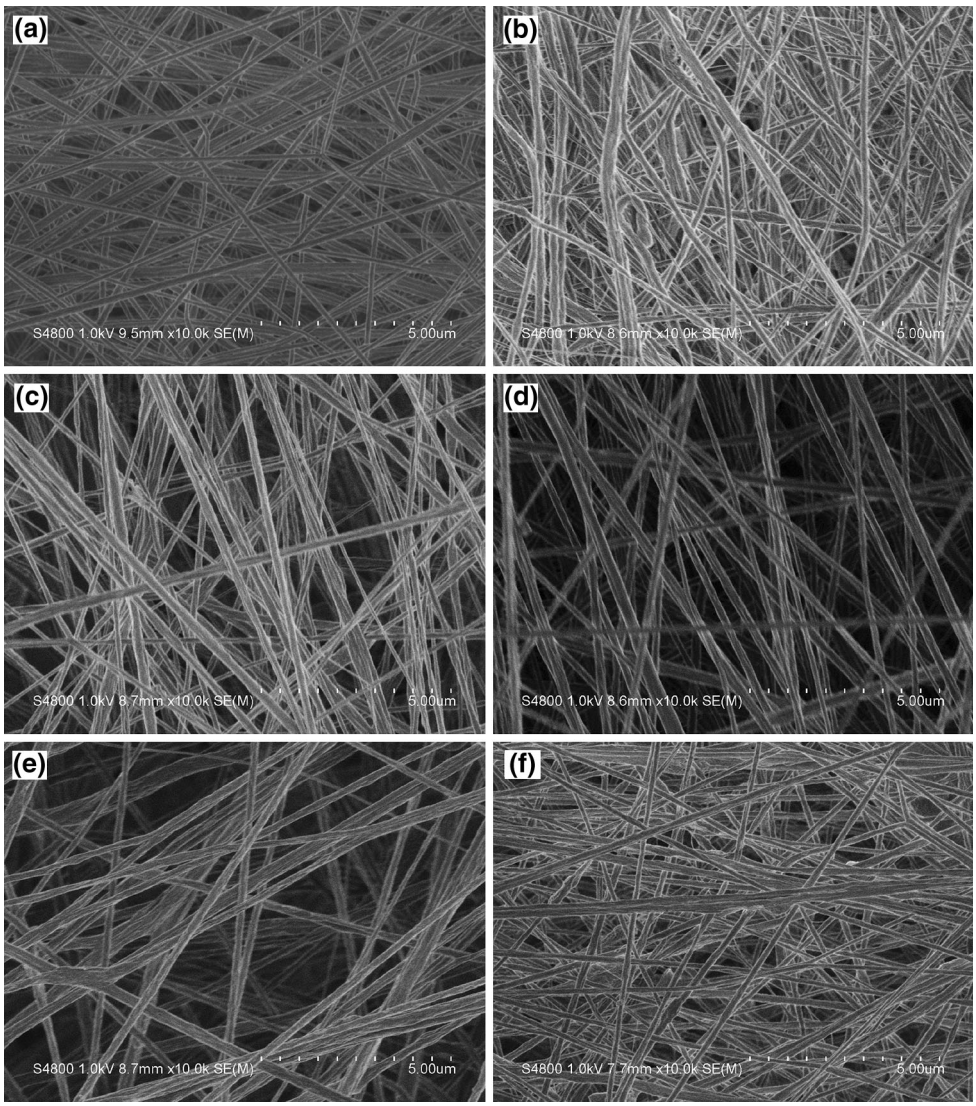

Fig. 4 FE-SEM images of electrospun nanofibers: **a** PAN, **b** MES/PAN, **c** MES/PAN/GO1, **d** MES/PAN/GO3, **e** MES/PAN/GO5 and **f** MES/PAN/GO10

molecular dispersed in electrospinning solution after the introducing of the GO nanosheets including intercalating into the interlayer spaces of multilayer GO nanosheets, covering on the surfaces of GO nanosheets and freedom movement. Figure 5 presents the schematic illustration representing the formation and evolution of the morphological structure for the electrospun PAN-based composite nanofibers with the addition of MES and GO. The remarkable improvement of interfacial interaction could be achieved with the increasing GO amounts in the composite nanofibers. Furthermore, the GO were well encapsulated and homogeneous dispersed in electrospun MES/PAN phase change composite nanofibers, which also demonstrated that the GO and MES/PAN composite component had good miscibility and excellent compatibility in those composite nanofibers. The FE-SEM image indicated that the electrospun PAN-based phase change composite nanofibers shows characteristic of form-stable PCMs without any leakage of the melted MES escaping from the nanofibers, which may be account for the three-dimensional network and nanospaces confinement effect of electrospun PAN nanofibers supporting skeleton, as well as the strong hydrogen bonding interaction confinement effect between the MES and PAN/GO supporting matrice. Therefore, the electrospun PAN-based phase change composite nanofibers with various GO loading can be considered as an innovative form-stable PCMs for the storage and retrieval of thermal energy.

Mechanical properties

The GO with extraordinary mechanical properties and very high aspect ratio is of the most effective nanofillers, which can effectively achieve the significant reinforcement in mechanical properties of polymer composites [36–47]. In order to investigate the reinforcing effect of GO in the PAN-based phase change composite nanofibers system, the mechanical behavior of electrospun PAN nanofibers, MES/

PAN, and MES/PAN/GO phase change composite nanofibers with different loadings of GO were studied by tensile testing. The typical stress–strain curves are shown in Fig. 6A and the corresponding averaged tensile strength and elongation at break of the all samples derived from the stress–strain curves are presented in Fig. 6B. As can be seen in Fig. 6A, the addition of MES into the electrospun PAN nanofibers led to a significant weakening of the mechanical properties, while the averaged tensile strength and elongation at break of electrospun MES/PAN phase change composite nanofibers were, respectively, decreased by 84 % (from 3.47 to 0.56 MPa) and 68 % (from 31.02 to 9.83 %) compared with those of pure PAN nanofibers because the MES acting as the dispersed phase could remarkably broke the continuous phase structure of electrospun PAN nanofibers. In addition, the lack of uniform morphological structure of electrospun MES/PAN phase change composite nanofibers with the coarse and wrinkled surfaces could also be responsible for the reduction of the mechanical properties. The results indicated that the loading of MES in the nanofibers was an unfavorable effect to the mechanical properties of the PAN-based phase change composite nanofibers and electrospun PAN nanofibers acting as the supporting materials provided a form-stable structure and mechanical strength for the phase change system. In contrast to the MES/PAN composite nanofibers, the mechanical performance of electropsun MES/PAN/GO phase change composite nanofibers was significantly improved due to the incorporation of the GO nanosheets. Figure 6B shows the averaged tensile strength of electropsun MES/PAN/GO phase change composite nanofibers increased continuously from 0.56 to 3.77 MPa with the increase of the GO amount in the nanofibers, indicating that the maximum tensile strength exhibited approximately 5.73 times increment compared to the MES/PAN phase change composite nanofibers. It could also be found from Fig. 6B that the elongation at the break showed gradually increased from 9.85 to 20.35 % with the adding of GO from 0 to 3 mass%, and then obviously decreased from 20.35 to 7.45 % as the further increasing GO loading from 3 to 10 mass%. The slight reduction of the elongation at break may be attributed to the restricted movement of the MES and PAN molecular chains during the tensile stretching due to the stronger interfacial interaction between different components, as well as slight aggregation and stacking of GO at higher content, which also demonstrated that the MES/PAN/GO phase change composite nanofibers showed more brittle failure (see Fig. 6A). The significant improvement of the mechanical properties can be contributed to the large aspect ratio, homogeneous dispersion of GO, and the strong interfacial interaction between GO and MES/PAN matrices. It was believed that the GO nanosheets with the high surface area had a beneficial effect on uniform distribution of stress concentration points in the composite nanofibers systems, suggesting that the external stress would be expected to transfer from the matrix to GO to avoid and minimize the presence of stress concentration center, resulting in significant enhancement of mechanical properties. The remarkable reinforcement of the mechanical properties also revealed that the GO

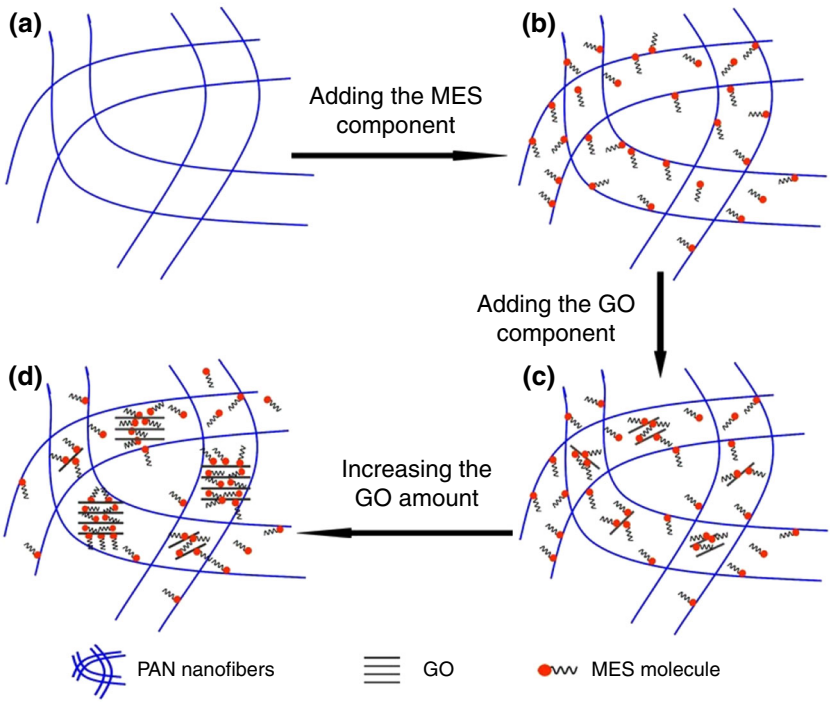

Fig. 5 Schematic representation showing the evolution of distribution of the MES component in the PAN-based phase change composite nanofibers with different GO amounts: **a** PAN, **b** MES/PAN, **c** MES/PAN/GO1, and **d** MES/PAN/GO10

nanosheets and MES/PAN matrices had good compatibility in those phase change composite nanofibers. The results from the tensile testing suggested that electropsun PAN-based phase change composite nanofibers with various GO amounts showed superior tensile properties, which could be competent and suitable for potential applications.

Thermal properties

DSC analysis

The phase change behaviors of the MES in the electrospun PAN-based phase change composite nanofibers and the effect of GO addition on the thermal energy storage, and release properties of electrospun MES/PAN/GO phase change composite nanofibers were investigated using DSC thermoanalytical technique. The representative DSC curves and corresponding thermal characteristic data of the extrapolated peak onset temperature (T_e), melting peak temperature (T_m), freezing peak temperature (T_c), melting enthalpy (ΔH_m), and freezing enthalpy (ΔH_c) are shown in Fig. 7 and Table 1, respectively. As revealed in Fig. 7, no phase transition peak was observed for the pure GO nanosheets and electrospun PAN nanofibers in the entire temperature region of the DSC analysis, suggesting that the GO and PAN supporting matrixes have no contribution to the phase change enthalpies of composite nanofibers. Apparently, there were the strongest endothermic and exothermic peaks representing the solid–liquid phase change behaviors of the pure MES powder. It was clearly seen that the intensity of endothermic and exothermic peaks for all electrospun PAN-based phase change composite nanofibers appeared to decrease compared to that of neat MES powders. It could also be observed from Fig. 7 and Table 1 that the T_e and T_c of electrospun MES/PAN and MES/PAN/GO phase change composite nanofibers with varying GO contents exhibited slightly decrease about 1–5 °C relative to those of the pristine MES powder. In addition, the ΔH_m and ΔH_c values of the MES/PAN phase change composite nanofibers were, respectively, lower than those of the MES powder, while the two enthalpies of the MES/PAN/GO phase change composite nanofibers also gradually decreased with the increase of GO content, which were mainly caused by the PAN and GO supporting matrixes significantly decreased the mass ratio of MES acting as solid–liquid PCMs for thermal energy storage and release in the whole phase change systems leading to the remarkably reduced heat enthalpies. It is notable that the ΔH_m and ΔH_c values of all composite nanofibers were nearly equal, which means that the PAN-based phase change composite nanofibers were a kind of transition reversible latent heat storage materials.

Moreover, it could be found that the experimental enthalpies extracting from DSC measurements were slightly lower than the theoretical enthalpies, which calculated by multiplying the enthalpy of pristine MES powder and the mass ratio of MES in the composite nanofibers. The efficiency of enthalpies (the ratio between the experimental value and the theoretical value) for the electrospun MES/PAN/GO phase change composite nanofibers with different GO loadings (0, 1, 3, 5, and 10 mass%) was 95.23/98.92, 98.53/99.35, 90.18/94.01, 88.32/92.00, and 91.52 %/95.26 %

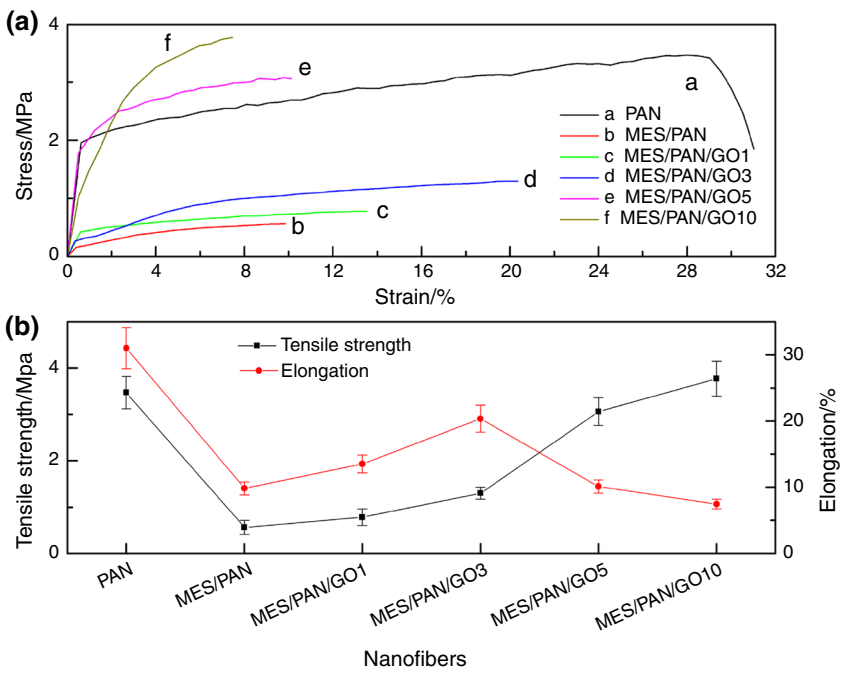

Fig. 6 **a** The typical stress–strain curves of electrospun PAN-based phase change composite nanofibers; **b** the corresponding curves with respect to tensile strength and elongation at break

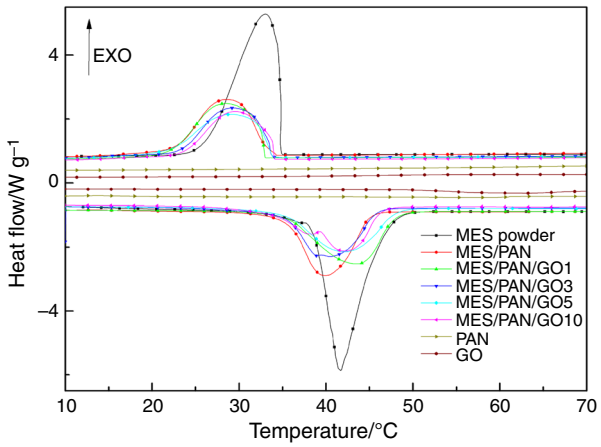

Fig. 7 DSC curves of pristine MES powder, electrospun PAN nanofibers and MES/PAN phase change composite nanofibers with various GO contents during **a** heating process and **b** cooling process

(melting/freezing), respectively. These results could be contributed to the retardation of the crystallization process for MES in the electrospun PAN-based phase change composite nanofibers and the crystallization being hindered as a result of the quench effect during electrospinning, the confinement effect of the three-dimensional network and nanoscaled phase change spaces, hydrogen bonding interactions, the dilution and shield supporting effect of GO and PAN supporting matrixes in the phase change system, which could substantially hamper the movement of MES molecules during the melting and freezing processes resulting in the difference of the experimental and the theoretical enthalpy value.

The enthalpy efficiency of the electrospun MES/PAN/GO phase change composite nanofibers slightly increases with the increase of GO in the phase change system, and then decreases. The increase of enthalpies efficiency for the electrospun MES/PAN/GO phase change composite nanofibers having low contents of GO may be attributed to the facilitation of MES crystallization in the composite nanofibers because the GO with high thermal conductivity could act as the nucleation agent and effectively promote the heterogeneous nucleation of MES. However, when concentration of GO was added, the GO with large specific surface area and interlayer structures also had strong adsorption effect on MES through capillary force and surface tension, and the intermolecular hydrogen bonding interactions were effectively improved resulting from numerous oxygen-containing functional groups attached on the surface of the GO nanosheets. In other word, the existence of the more strong interfacial interaction between MES, GO, and PAN polymeric matrix may also increase the molecular entanglement and impede the freedom mobility of MES molecules chains, resulting in the suppression of the crystallization of MES and further leading to the decreased enthalpy efficiency. It was noteworthy that the confined conformation of the MES molecules in special nanoscaled phase change spaces may be different from the curving and freedom conformation of MES molecule chains in the bulk systems. Moreover, it is also believed that the thermal energy of the phase transition could not destroy the confinement effect of strong interfacial interaction, while the MES in the composite nanofibers system hardly crystallized as the temperature was decreased to the T_c of pristine MES powder. Therefore, the freezing temperatures of electrospun PAN-based phase change composite nanofibers slightly decrease compared with those of the neat MES powder.

Meanwhile, the thermal reliability of the electrsopun MES/PET/GO5 phase change composite nanofibers after thermal cycling were also determined, and the DSC thermal cycle curves are show in Fig. 8. It can be obviously observed from Fig. 8 that the composite nanofibers showed reversible thermal storage and release processes, and the intensity of melting and freezing peaks had no distinguishable variations during the heating and cooling processes, which was meant that electrospun PAN-based phase change composite nanofibers had good thermal reliability properties and can be implemented to transfer energy in different time and space.

Table 1 The peak onset temperature (T_e), melting peak temperature (T_m), freezing peak temperature (T_c), melting enthalpy (ΔH_m), and freezing enthalpy (ΔH_c) of neat MES powder and electrospun PAN-based phase change composite nanofibers

Samples	Melting			Freezing		
	T_e/°C	T_m/°C	ΔH_m/kJ kg^{-1}	T_e/°C	T_c/°C	ΔH_c/kJ kg^{-1}
MES	38.66	41.69	205.4	34.95	33.02	197.2
MES/PAN	35.49	39.96	106.7	33.28	28.39	106.4
MES/PAN/GO1	34.96	43.53	109.3	32.98	28.38	105.8
MES/PAN/GO3	35.11	40.44	98.10	33.67	29.14	98.08
MES/PAN/GO5	34.94	42.02	94.80	33.82	28.95	94.01
MES/PAN/GO10	37.38	42.20	92.27	34.04	29.48	92.23

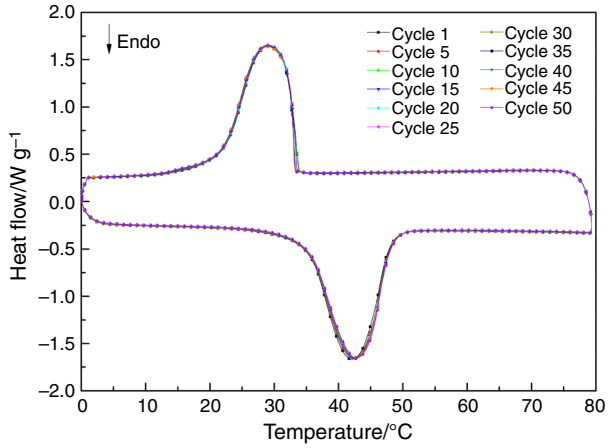

Fig. 8 DSC cycle curves of electrospun MES/PAN/GO5 phase change composite nanofibers

TG analysis

The thermal stability of pristine MES powder, GO, electrospun PAN nanofibers, and MES/PAN/GO phase change composite nanofibers with different GO amounts was studied by thermogravimetric analysis (TG). The thermogravimetric (TG) and differential thermogravimetric (DTG) curves are shown in Fig. 9. The data of the extrapolated 5 mass% mass loss temperature ($T_{-5\ \mathrm{mass\%}}$), the maximum decomposition temperatures (T_{max1} and T_{max2}) and the charred residue amount at 800 °C are tabulated in Table 2. Figure 9 shows that electrospun PAN nanofibers underwent a one-step decomposition process occurring roughly at 322–534 °C, resulting from the thermal degradation of the PAN molecular chains. The pure MES powder started to be degradation at about 170 °C, and the final mass loss percentage was nearly 100 % at 800 °C. Apparently, the thermal decomposition temperature range of electrospun PAN nanofibers was significantly higher than that of the MES powder, suggesting that the PAN nanofibers had excellent thermal stability and could act as the supporting materials for the preparation of form-stable phase change composite nanofibers. It was also obviously observed from Fig. 9 that there were two less mass loss steps for the GO at temperature of 67–318 °C. The first slight mass loss at temperature below 110 °C was about 7 mass%, which can be typically attributed to the evaporation of absorbed water on the surface of GO. The second mass loss at about 200–318 °C was due to the removal of labile oxygen-containing functional groups such as hydroxyl, epoxide, carboxyl, and carbonyl groups [38–46]. As can be seen in Fig. 9, the two dramatic thermal degradation processes of electrospun MES/PAN phase change composite nanofibers were clearly observed with the increasing temperature. The mass loss was about 51 % between 173 and 280 °C, belonging to the decomposition of the MES in the composite nanofibers, and the other mass loss from 326 to 472 °C was about 31 %, ascribed to the thermal degradation of the PAN supporting matrixes. As revealed in Table 2, the $T_{-5\ \mathrm{mass\%}}$ and the charred residue amount at 800 °C of the electrospun MES/PAN phase change composite nanofibers obviously increased about 15 °C and 10.2 mass%, respectively, compared to the pure MES powder due to the polymer protection and supporting effect of the PAN nanofibers with the good thermal stability. For the electrospun MES/PAN/GO phase change composite nanofibers with various GO contents, the similar two stages mass loss behaviors were also recorded during the TG measurements. The first stage of the mass loss taking place in the region of about 180–280 °C was mainly assigned to the degradation of the MES molecular chains in the composite nanofibers. The corresponding mass loss was about 47 mass% for the MES/PAN/GO3, 45 mass% for the MES/PAN/GO5, and 40 mass% for the MES/PAN/GO10, respectively. The second stage happened approximately at 300–470 °C and the mass loss was about 32 %, corresponding to the degradation of the PAN molecular chains. The results from Fig. 9 and Table 2 indicated that the mass loss of electrospun MES/PET/GO phase change composite nanofibers gradually decreased as the increasing GO loading during the first thermal degradation stage, which could be mainly explained by the reduced mass ratios of MES in the composite nanofibers due to the addition of GO. In addition, as shown in inset magnified image of Fig. 9a, the $T_{-5\ \mathrm{mass\%}}$ of electrospun MES/PAN/GO phase change composite nanofibers slightly shifted to the higher temperature, which was, respectively, about 5, 8, and 10 °C increment for the MES/PAN/GO3, MES/PAN/GO5, and MES/PAN/GO10 in contrast to that of MES/PAN composite nanofibers (see Table 2). This result could be contributed to the fact that the mobility of the MES molecular chains at the interfaces of PAN and GO could be suppressed by the stronger interfacial interactions owing to increasing incorporation of the GO. And the GO embedding in the composite nanofibers possibly also created a physical protective shield to delaying the thermal decomposition of MES. Moreover, Table 2 presents that the charred residue amount at 800 °C also significantly increased with the increase of the GO content compared with that of the MES/PAN composite nanofibers, suggesting that the introduction of GO into phase change composite nanofibers remarkably enhanced the formation of char at the high temperature by creating the thermal physical protective barrier, leading to the reduction of the thermal mass loss. The TG results showed that the remarkable improvement of the thermal stability for electrospun PAN-based phase change composite nanofibers could be effectively achieved by loading GO into

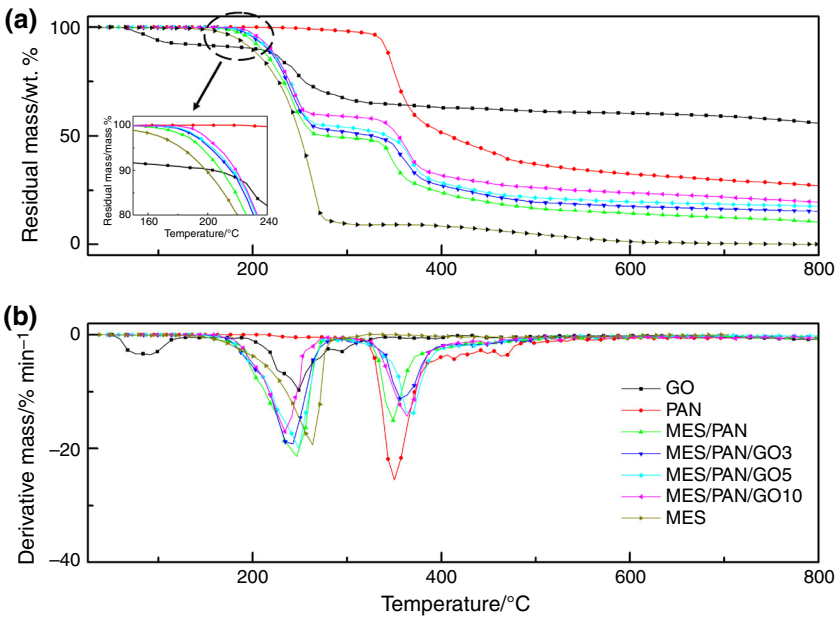

Fig. 9 TG (**a**) and DTG (**b**) curves of pristine MES powder, GO, electrospun PAN nanofibers, and the PAN-based phase change composite nanofibers. The *inset* in **a** displays the magnified thermal degradation curves of first stage

Table 2 The characteristic temperatures and charred residue amount of the MES powder, GO, electrospun PAN nanofibers, and phase change composite nanofibers

Samples	$T_{-5\ mass\%}$/°C	T_{max1}/°C	T_{max2}/°C	Charred residue/mass%
GO	92.31	91.31	248.66	55.95
PAN	333.29	–	350.34	27.29
MES/PAN	195.99	246.70	348.77	10.30
MES/PAN/GO3	200.31	242.40	356.11	15.27
MES/PAN/GO5	203.31	248.62	370.33	17.66
MES/PAN/GO10	205.67	233.89	363.64	19.61
MES powder	180.82	263.55	–	0.03

composite nanofibers as a result of the reinforced interfacial interactions and the thermal physical protective barrier effect.

Thermal energy storage and release performance

Thermal energy storage and release performance of form-stable phase change composite nanofibers is one of the particularly important characteristics that could obviously affect the heat transfer in thermal storage applications. In order to improve the thermal conductivity of electrospun MES/PAN phase change composite nanofibers, the GO was added to the composite nanofibers with different mass fraction. The effect of GO additive on thermal energy storage and release rates of the electrospun MES/PAN phase change composite nanofibers was investigated, and the typical heating and cooling temperature curves of the neat MES powders, MES/PAN, and MES/PAN/GO composite nanofibers with different GO contents are, respectively, shown in Fig. 10a, b. Figure 10 reveals that the electrospun MES/PAN phase change composite nanofibers with GO additive had higher heating and cooling rates than those of the MES/PAN phase change composite nanofibers. In addition, the heat storage and release rates of the MES/PAN/GO phase change composite nanofibers remarkably increased with the increase of GO contents during phase change processes. The melting time was determined from the heating curve as the time from the same initial temperature at about 15 °C to the melting peak temperature of the samples at approximately 41 °C. Similarly, the interval time between the same initial temperature (about 55 °C) and the freezing peak temperature of the samples (about 29 °C) was defined as the freezing time from the cooling curve. As seen from Fig. 10a, when the temperature rises from 15 to 41 °C, it takes about 6.8, 3.8, and 2.8 min for the MES/PAN, MES/PAN/GO5, and MES/PAN/GO10 phase change composite nanofibers, respectively. Apparently, the melting times of the electrospun MES/PAN/GO phase change composite nanofibers with 5 and 10 mass% GO contents were, respectively, decreased by 44 and 59 % in comparison with that of the MES/PAN phase change composite nanofibers without GO loading. Moreover, it could be found from Fig. 10b that the freezing times of the MES/PAN, MES/PAN/GO5, and MES/PAN/GO10 phase change composite nanofibers were determined as 7.5, 4.3, and 2.7 min, suggesting the corresponding freezing times were, respectively, reduced about 43 and 64 % as compared to that of MES/PAN. These results suggested that the heat transfer rate and/or convection of MES in MES/PAN/GO phase change composite nanofibers were significantly

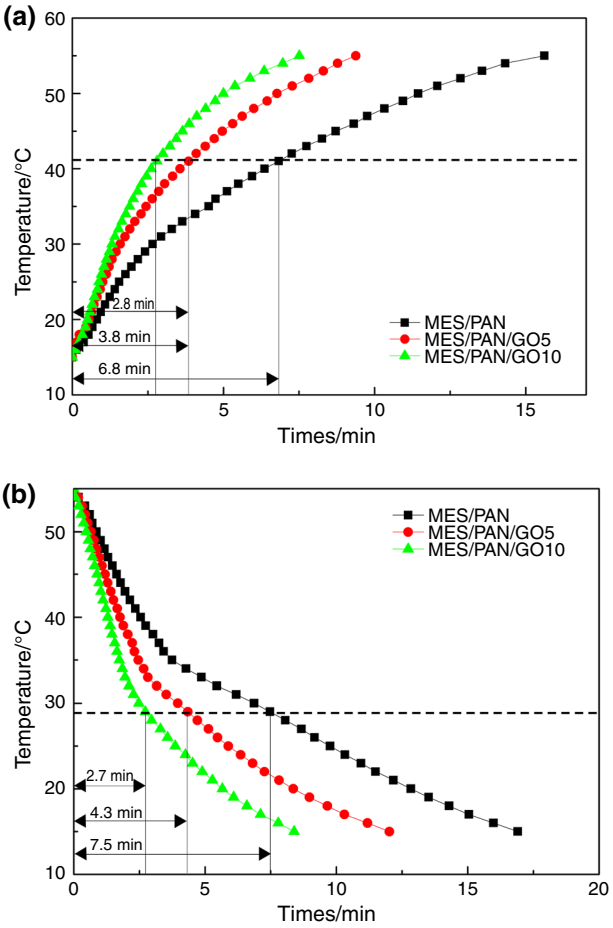

Fig. 10 Heat storage and release curves of electrospun MES/PAN, MES/PAN/GO5, and MES/PAN/GO10 phase change composite nanofibers: **a** heat storage and **b** heat release

enhanced by introducing GO due to the excellent thermal conductivity ability of GO and the formation of continuous heat conducting network as a result of the homogeneous dispersion., In other words, the GO nanosheets acting as heat conductive bridges could remarkably contributed to form an efficient percolating path for heat flow in the electrospun MES/PAN/GO phase change composites nanofibers, leading to the decrease in melting and freezing times of the MES/PAN/GO composite nanofibers.

Conclusions

In this work, an innovative type of electrospun MES/PAN phase change composite nanofibers with different GO loading was prepared by electrospinning. The FT-IR results revealed that there was an excellent compatibility between MES molecular and PAN/GO supporting matrices and the strengthened interfacial interactions could effectively prevent the leakage of melted MES from the PAN/GO supporting skeleton. The observations by FE-SEM indicated that the GO nanosheets could be well dispersed and wrapped in electrospun MES/PAN/GO phase change composite nanofibers, which presented coarse and rough morphological structures with an average diameter of about 200 nm. In addition, the results also suggested that adding GO nanosheets have beneficial effect on mechanical properties, thermal stability, and thermal energy storage and release performances of the electrospun PAN-based phase change composite nanofibers. The DSC analysis indicated that the electrospun phase change composite nanofibers had reversible phase change behaviors and could effectively control heat storage and release of MES in the supporting matrix. Moreover, Results of the DSC thermal cycling suggested that the electrospun MES/PAN/GO phase change composite nanofibers exhibit excellent cyclic reliability performances after undergoing the highly reversible phase transformation of 50 times. The significant enhancement of thermal energy storage and release rates was also confirmed by comparing the melting/freezing times of electrospun MES/PAN/GO and MES/PAN phase change composite nanofibers. The present research provides a novel PAN-based form-stabled composite PCMs with the excellent thermal and mechanical properties for the applications related to storage and retrieval of thermal energy such as energy efficient buildings, thermo-regulating fibers, thermal protection, etc.

Acknowledgements This research was financially supported by the National High-tech R&D Program of China (No. 2012AA030313), Changjiang Scholars and Innovative Research Team in University (No. IRT1135), National Natural Science Foundation of China (No. 51006046 and No. 51163014), the Priority Academic Program Development of Jiangsu Higher Education Institutions, Industry-Academia-Research Joint Innovation Fund of Jiangsu Province (BY2012068), and Science and Technology Support Program of Jiangsu Province (SBE201201094).

References

1. Tyagi VV, Kaushika SC, Tyagib SK, Akiyamac T. Development of phase change materials based microencapsulated technology for buildings: a review. Renew Sust Energy Rev. 2011;15:1373–91.
2. Ozturk HH. Experimental evaluation of energy and energy efficiency of a seasonal latent heat storage system for greenhouse heating. Energy Convers Manag. 2005;46:1523–42.
3. Wang YH, Yang YT. Three-dimensional transient cooling simulations of a portable electronic device using phase change materials (PCM) in multi-fin heat sink. Energy. 2011;36:5214–24.
4. Rossi RM, Bolli WP. Phase change materials for improvement of heat protection. Adv Eng Mater. 2005;7:368–73.
5. Regin AF, Solanki SC, Saini JS. Heat transfer characteristics of thermal energy storage system using PCM capsules: a review. Renew Sust Energy Rev. 2008;12:2438–58.
6. Ren N, Wu YT, Wang T, Ma CF. Experimental study on optimized composition of mixed carbonate for phase change thermal storage in solar thermal power plant. J Therm Anal Calorim. 2011;104:1201–8.

7. Wu SM, Fang GY. Dynamic performances of solar heat storage system with packed bed using myristic acid as phase change material. Energy Build. 2011;43:1091–6.
8. Varuna PV, Singal SK. Review of mathematical modeling on latent heat thermal energy storage systems using phase-change material. Renew Sust Energy Rev. 2008;12:999–1031.
9. Aydin AA, Okutan H. High-chain fatty acid esters of myristyl alcohol with odd carbon number: novel organic phase change materials for thermal energy storage—2. Sol Energy Mater Sol Cells. 2011;95:2417–23.
10. Sarı A, Biçer A, Karaipekli A. Synthesis, characterization, thermal properties of a series of stearic acid esters as novel solid–liquid phase change materials. Mater Lett. 2009;63:1213–6.
11. Sari A, Bicer A, Karaipekli A, Alkan C, Karadag A. Synthesis, thermal energy storage properties and thermal reliability of some fatty acid esters with glycerol as novel solid–liquid phase change materials. Sol Energy Mater Sol Cells. 2010;94:1711–5.
12. De Santis R, Ambrogi V, Carfagna C, Ambrosio L, Nicolais L. Effect of microencapsulated phase change materials on the thermo-mechanical properties of poly(methyl-methacrylate) based biomaterials. J Mater Sci Mater Med. 2006;17:1219–26.
13. Cai YB, Wei QF, Huang FL, Lin SL, Chen F, Gao WD. Thermal stability, latent heat and flame retardant properties of the thermal energy storage phase change materials based on paraffin/high density polyethylene composites. Renew Energy. 2009;34:2117–23.
14. Zukowski M. Experimental study of short term thermal energy storage unit based on enclosed phase change material in polyethylene film bag. Energy Convers Manag. 2007;48:166–73.
15. Mochane MJ, Luyt AS. Preparation and properties of polystyrene encapsulated paraffin wax as possible phase change material in a polypropylene matrix. Thermochim Acta. 2012;544:63–70.
16. Beginn U. Applicability of frozen gels from ultra high molecular weight polyethylene and paraffin waxes as shape persistent solid/liquid phase change materials. Macromol Mater Eng. 2003;288:245–51.
17. Pielichowski K, Flejtuch K. Binary blends of polyethers with fatty acids: a thermal characterization of the phase transitions. J Appl Polym Sci. 2003;90:861–70.
18. Sari A, Alkan C. Preparation and thermal energy storage properties of poly(*n*-butyl methacrylate)/fatty acids composites as form-stable phase change materials. Polym Compos. 2012;33:92–8.
19. Guo YQ, Tong Z, Chen MC, Liang XH. Solution miscibility and phase-change behavior of a polyethylene glycol-diacetate cellulose composite. J Appl Polym Sci. 2003;88:652–8.
20. Alkan C, Gunther E, Hiebler S, Himpel M. Complexing blends of polyacrylic acid-polyethylene glycol and poly(ethylene-co-acrylic acid)-polyethylene glycol as shape stabilized phase change materials. Energy Convers Manag. 2012;64:364–70.
21. Sarier N, Onder E. Thermal characteristics of polyurethane foams incorporated with phase change materials. Thermochim Acta. 2007;454:90–8.
22. Ma YH, Chu XD, Li W, Tang GY. Preparation and characterization of poly(methyl methacrylate-co-divinylbenzene) microcapsules containing phase change temperature adjustable binary core materials. Sol Energy. 2012;86:2056–66.
23. Cai YB, Gao CT, Xu XL, Fu Z, Fei XZ, Zhao Y, Chen Q, Liu XZ, Wei QF, He GF, Fong H. Electrospun ultrafine composite fibers consisting of lauric acid and polyamide 6 as form-stable phase change materials for storage and retrieval of solar thermal energy. Sol Energy Mater Sol Cells. 2012;103:53–61.
24. Chen CZ, Wang LG, Huang Y. A novel shape-stabilized PCM: electrospun ultrafine fibers based on lauric acid/polyethylene terephthalate composite. Mater Lett. 2008;62:3515–7.
25. Li M, Wu ZS, Kao HT. Study on preparation, structure and thermal energy storage property of capric-palmitic acid/attapulgite composite phase change materials. Appl Energy. 2011;88:3125–32.
26. Wang WL, Yang XX, Fang YT, Ding J. Preparation and performance of form-stable polyethylene glycol/silicon dioxide composites as solid–liquid phase change materials. Appl Energy. 2009;86:170–4.
27. Karaman S, Karaipekli A, Sari A, Bicer A. Polyethylene glycol (PEG)/diatomite composite as a novel form-stable phase change material for thermal energy storage. Sol Energy Mater Sol Cells. 2011;95:1647–53.
28. Mei DD, Zhang B, Liu RC, Zhang YT, Liu JD. Preparation of capric acid/halloysite nanotube composite as form-stable phase change material for thermal energy storage. Sol Energy Mater Sol Cells. 2011;95:2772–7.
29. Karaipekli A, Sari A. Capric-myristic acid/expanded perlite composite as form-stable phase change material for latent heat thermal energy storage. Renew Energy. 2008;33:2599–605.
30. Karaipekli A, Sari A. Preparation, thermal properties and thermal reliability of eutectic mixtures of fatty acids/expanded vermiculite as novel form-stable composites for energy storage. J Ind Eng Chem. 2010;16:767–73.
31. Kao HT, Li M, Lv XW, Tan JM. Preparation and thermal properties of expanded graphite/paraffin/organic montmorillonite composite phase change material. J Therm Anal Calorim. 2012;107:299–303.
32. Meng X, Zhang HZ, Sun LX, Xu F, Jiao QZ, Zhao ZM, Zhang J, Zhou HY, Sawada Y, Liu YL. Preparation and thermal properties of fatty acids/CNTs composite as shape-stabilized phase change materials. J Therm Anal Calorim. 2013;111:377–84.
33. Cui YB, Liu CH, Hu S, Yu X. The experimental exploration of carbon nanofiber and carbon nanotube additives on thermal behavior of phase change materials. Sol Energy Mater Sol Cells. 2011;95:1208–12.
34. Zeng JL, Cao Z, Yang DW, Sun LX, Zhang L. Thermal conductivity enhancement of Ag nanowires on an organic phase change material. J Therm Anal Calorim. 2010;101:385–9.
35. Zhu YW, Murali S, Cai WW, Li XS, Suk JW, Potts JR, Ruoff RS. Graphene and graphene oxide: synthesis, properties, and applications. Adv Mater. 2010;22:3906–24.
36. Xu Z, Gao C. In situ polymerization approach to graphene-reinforced nylon-6 composites. Macromolecules. 2010;43:6716–23.
37. Rodríguez-Gonzalez C, Martínez-Hernandez AL, Castano VM, Kharissova OV, Ruoff RS, Velasco-Santos C. Polysaccharide nanocomposites reinforced with graphene oxide and keratin-grafted graphene oxide. Ind Eng Chem Res. 2012;51:3619–29.
38. Xu YX, Hong WJ, Bai H, Li C, Shi GQ. Strong and ductile poly(vinyl alcohol)/graphene oxide composite films with a layered structure. Carbon. 2009;47:3538–43.
39. Cao YW, Zhang J, Feng JC, Wu PY. Compatibilization of immiscible polymer blends using graphene oxide sheets. ACS Nano. 2011;5:5920–7.
40. Zhan YQ, Yang XL, Guo H, Yang J, Meng FB, Liu XB. Cross-linkable nitrile functionalized graphene oxide/poly(arylene ether nitrile) nanocomposite films with high mechanical strength and thermal stability. J Mater Chem. 2012;22:5602–8.
41. Wang Y, Shi ZX, Fang JH, Xu HJ, Yin J. Graphene oxide/polybenzimidazole composites fabricated by a solvent-exchange method. Carbon. 2011;49:1199–207.
42. Wang JY, Jia HB, Tang YY, Ji DD, Sun Y, Gong XD, Ding LF. Enhancements of the mechanical properties and thermal conductivity of carboxylated acrylonitrile butadiene rubber with the addition of graphene oxide. J Mater Sci. 2013;48:1571–7.
43. Ma WS, Li J, Zhao XS. Improving the thermal and mechanical properties of silicone polymer by incorporating functionalized graphene oxide. J Mater Sci. 2013;48:5287–94.
44. Tseng IH, Chang JC, Huang SL, Tsai MH. Enhanced thermal conductivity and dimensional stability of flexible polyimide nanocomposite film by addition of functionalized graphene oxide. Polym Int. 2013;62:827–35.

45. Wang JY, Jia HB, Tang YY, Ji DD, Sun Y, Gong XD, Ding LF. Enhancements of the mechanical properties and thermal conductivity of carboxylated acrylonitrile butadiene rubber with the addition of graphene oxide. J Mater Chem. 2011;21:4222–7.
46. Li YL, Kuan CF, Chen CH, Kuan HC, Yip MC, Chiu SL, Chiang CL. Preparation, thermal stability and electrical properties of PMMA/functionalized graphene oxide nanosheets composites. Mater Chem Phys. 2012;134:677–85.
47. Huang YJ, Qin YW, Zhou Y, Niu H, Yu ZZ, Dong JY. Polypropylene/graphene oxide nanocomposites prepared by in situ Ziegler–Natta polymerization. Chem Mater. 2010;22:4096–102.
48. Fabbri P, Valentini L, Bittolo Bon S, Foix D, Pasquali L, Montecchi M, Sangermano M. In-situ graphene oxide reduction during UV-photopolymerization of graphene oxide/acrylic resins mixtures. Polymer. 2012;53:6039–44.
49. Bora C, Dolui SK. Fabrication of polypyrrole/graphene oxide nanocomposites by liquid/liquid interfacial polymerization and evaluation of their optical, electrical and electrochemical properties. Polymer. 2012;53:923–32.
50. Yan XB, Chen JT, Yang J, Xue QJ, Miele P. Fabrication of free-standing, electrochemically active, and biocompatible graphene oxide-polyaniline and graphene-polyaniline hybrid papers. ACS Appl Mater Interface. 2010;2:2521–9.
51. Shen XJ, Pei XQ, Fu SY, Friedrich K. Significantly modified tribological performance of epoxy nanocomposites at very low graphene oxide content. Polymer. 2013;54:1234–42.
52. Ma GP, Yang DZ, Nie J. Preparation of porous ultrafine polyacrylonitrile (PAN) fibers by electrospinning. Polym Adv Technol. 2009;20:147–50.